THE JOURNAL OF PHYSICAL CHEMISTRY B

ARTICLE

pubs.acs.org/JPCB

DNA Cyclization: Suppression or Enhancement by Electrostatic Repulsions?

A. G. Cherstvy

Institute of Complex Systems, ICS-2, Theoretical Soft Matter and Biophysics, Forschungszentrum Jülich, 52425 Jülich, Germany

ABSTRACT: First, we develop a model of counterion condensation on highly charged polyelectrolyte rings. Using the known analytical results for the electrostatic energy of ring formation, a stronger counterion adsorption is anticipated onto a cyclized polyelectrolyte, as compared to the Manning prediction for a straight rod-like polyelectrolyte. This fact ensures a lower energetic cost of polyelectrolyte bending into a ring. In the main part of the work, we investigate the impact of charges on cyclization of short DNA fragments, both theoretically and by computer simulations. An approximate expression for the electrostatically renormalized DNA cyclization probability is proposed that incorporates the electrostatic energies of polyelectrolyte cyclization and dimerization reactions. Depending on concentration of simple salt and chain length, the probability of formation of ideal polyelectrolyte rings can be either electrostatically inhibited or enhanced. The latter effect is quite counterintuitive. Afterward, simple computer simulations are performed to enumerate the effects of DNA thermal fluctuations onto the electrostatic energies of cyclized and dimerized DNA fragments in solution. Their outcomes support the possibility of electrostatically enhanced polyelectrolyte ring formation reaction in solution. In the end, we discuss some implications of the results obtained for the future DNA cyclization experiments and provide a short analysis of possible DNA-related features neglected in the modeling.

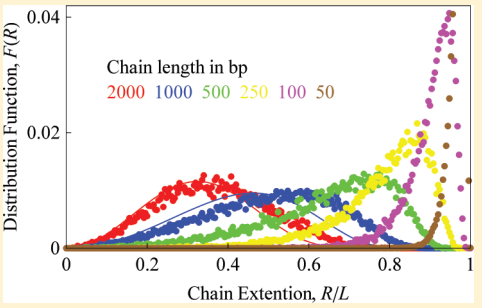

1. INTRODUCTION

DNA looping plays a vital role in a number of biochemical processes, including transcriptional regulation of genes,[1,2] the formation and functioning of DNA−protein complexes[3−7] and DNA wrapping in nucleosomes.[8] For highly negatively charged DNA molecules, the total cost of deformations comprises the mechanical deformation energy of its backbone and the energy of charge−charge interactions that crucially depends on the amount and type of salt added into the solution. This electrostatic (ES) energy scales as the square of DNA residual charge, counted after the accumulation of positive cations near the DNA surface. Charge renormalization and counterion condensation (CC) phenomena are well studied for a straight thin polyelectrolyte (PE) chain in low-salt solutions.[9−11] The degree of CC on weakly bent PEs is expected to be stronger than on straight ones,[12,13] while for the CC onto PE rings[14−16] no self-consistent analytical theory has been proposed so far, to the best of our knowledge.

Ligase-assisted DNA cyclization is a well-established technique for measuring the bending and twisting characteristics of DNA fragments of 100−5000 base pairs (bp) in length. The probability of DNA cyclization in solution characterized by the *J*-factor has been monitored under the controlled salt conditions in a number of experimental studies.[17−25] During the ligation process, DNA fragments with bp-complementary spatially proximal ends are "trapped" via the end-closure-reaction mediated by a specific enzyme joining the DNA strands together, the T4 bacteriophage DNA ligase. This joining gives rise to the formation of DNA circles and dimers in solution. The cyclization *J*-factor is then defined as the ratio of equilibrium constants of unimolecular ring formation reaction K_1 and bimolecular dimerization reaction K_2, namely $J = K_1/K_2$. The same is true for the kinetic rate constants of the corresponding reactions, $k_{1,2}$.[26] Theoretical calculations of the ring formation probabilities by uncharged semiflexible chains[27−33] as well as some more recent computer simulations[34,35] have revealed a relatively good agreement with the experimental data available for ∼300−2000 bp DNA fragments in the standard buffer.

For ∼80−120 bp short DNA fragments forming DNA minicircles, however, the cyclization factor reported recently[21,24] appears to be several orders of magnitude higher than predicted by the Shimada−Yamakawa (SY) theory.[30] The effect is particularly pronounced (with up to 10^5 (!) times higher *J*-factors) for easily bendable DNA fragments that reveal a strong affinity to histone proteins in nucleosomes, the so-called DNA nucleosome positioning sequences. The abnormally high DNA flexibility on small length-scales detected recently[36] can serve as a tentative explanation for this intriguing phenomenon. Another possible reason is a DNA "softening" that can be triggered by divalent Mg^{2+} cations present at ∼1−10 mM concentrations in all DNA ligation buffers. This effect is known to occur both for DNAs in solution[37] and for DNAs adsorbed on positively charged

Received: January 12, 2011
Revised: February 17, 2011
Published: March 29, 2011

surfaces.[38] Note here that some disagreement on the *J*-values for ~100 bp DNA fragments still exists in the experimental literature[21,22,39] and more precise equilibrium measurements of DNA ring closure reaction should clarify this issue in the future.

Physically, particularly at low simple-salt concentrations n_0, the DNA cyclization factor should be affected by the strength of CC and ES DNA ring formation energy. In particular, at lower n_0 values, the formation of DNA circles is expected to be inhibited due to a larger overall DNA bending stiffness. The effect of added 1:1 salt onto the *J*-factor has however not been studied systematically, except for a single experimental investigation reported in ref 20. Surprisingly, this study has revealed no detectable changes in the *J*-factor for n_0 = 3−160 mM of NaCl added and for $L \approx$ 350 bp DNA fragments. In this situation, one could expect that larger n_0 levels should reduce the total DNA bending persistence length l_p, thereby facilitating the DNA cyclization (larger *J* values). On the contrary, the l_p values extracted from the cyclization data were shown to *increase* slightly with increasing the amount of simple salt.[20] It was suggested that at higher n_0 levels, the Mg^{2+}cations bound to DNA are exchanged for Na^+, that are likely to be less effective in neutralizing the DNA charge. Therefore, the ES contribution to the DNA persistence length might effectively grow.

This work is organized as follows. First, we consider the CC onto ideal polyelectrolyte (PE) rings within a simple model, calculating the ES free energy of the ring formation. Using these results and an expression for the length-dependent PE persistence length, we rationalize the ES effects onto ring formation probabilities by weakly fluctuating PE chains, as a model for DNA cyclization in solution. The approach is based on simple modifications of the SY theory that account for the ES effects. Then, we analyze the outcomes of computer simulations that have been performed to assess the energy of the ring closure and dimerization of fluctuating PE fragments in solution. Some implications of these results for DNA cyclization experiments are discussed at the end.

2. COUNTERION CONDENSATION ONTO POLYELECTROLYTE RINGS

We consider a negative uniformly charged PE chain with screened Debye−Hückel repulsive potentials acting between its monomers, as a model for ES behavior of DNA molecules in solution. The case of monovalent cations is treated only, with no attraction between PE segments possible. Below, the analytical expressions for the ES cyclization energy[15] are employed in order to infer the CC degree on highly charged DNA-like PE chains upon ring formation. We neglect here the DNA helicity effects on the degree of CC that were shown to be small for a straight helical PE.[10]

The free energy functional $\Delta G(L)$ for the ring formation by a linear PE of the length $L = 2\pi R'$ with the adsorbed counterions can be written in the form similar to that for weakly bent semiflexible PEs:[12]

$$\Delta G(L) = \frac{l_B}{2b^2}[\alpha_c^2\varepsilon_c(L) - \alpha_r^2\varepsilon_r(L)] + \frac{k_BTL}{b}[\alpha_c \ln \alpha_c + (1-\alpha_c)\ln(1-\alpha_c) - \alpha_r \ln \alpha_r - (1-\alpha_r)\ln(1-\alpha_r)] + \frac{k_BTL}{b}(\alpha_c - \alpha_r)\ln A \quad (1)$$

Here $l_B = e_0^2/(\varepsilon k_BT) \approx 7$ Å is the Bjerrum length (e_0 is the elementary charge, ε is the dielectric constant of water, and k_BT is the thermal energy), $1/b$ is the linear density of PE adsorption sites, and $\alpha_{r,c}$ is the fraction of non-neutralized PE charge. The latter is assumed to be constant along the PE (PE end effects are neglected). The subscripts *c* and *r* correspond to the circle and rod quantities. The first term in eq 1 is the ES energy of PE ring formation, ΔE. The second one is the lattice-gas-like mixing free energy of noninteracting cations adsorbed on PE monomers. The last term describes the chemical potential and activity *A* of cations.

For situations when the PE charge density α/b remains constant, the ES ring formation energy is given by the first term of eq 1, namely

$$\Delta E(L) = \frac{l_B\alpha^2}{2b^2}[\varepsilon_c(L) - \varepsilon_r(L)] \quad (2)$$

For long PEs, it approaches the ES energy required to connect two infinitely long PE rods into one, the so-called ES closure energy,[15]

$$E_{cl} = \frac{k_BTl_B\alpha^2}{\kappa b^2} \quad (3)$$

The ES energies $E(L) = l_B\alpha^2\varepsilon(L)/(2b^2)$ that are stored in the circle and rod are, respectively:[15]

$$\frac{E_c(L)}{k_BT} = \frac{l_B\alpha^2}{2b^2}\left(-(2\pi R')^2\kappa_1 F_2\left[\left\{\frac{1}{2}\right\}, \left\{1, \frac{3}{2}\right\}, (\kappa R')^2\right] + (2\pi R')^3\frac{\kappa^2}{\pi^2}{}_2F_3\left[\{1,1\}, \left\{\frac{3}{2}, \frac{3}{2}, 2\right\}, (\kappa R')^2\right] - 2L\ln\frac{\pi a}{2L}\right) \quad (4)$$

$$\frac{E_r(L)}{k_BT} = \frac{l_B\alpha^2}{2b^2}\left(-\frac{2}{\kappa}[1 - e^{-\kappa L} - \kappa L Ei(-\kappa L)] + 2L[-\ln \kappa L - \gamma + 1] + 2L\left[\ln\frac{L}{a} - 1\right]\right) \quad (5)$$

Here $1/\kappa = \lambda_D = 1/(8\pi l_B n_0)^{1/2}$ is the Debye screening length, $Ei(-x) = \int dx e^{-x}/x$ is the exponential integral, *F* is the generalized hypergeometric function, and $\gamma \approx 0.577$. Also, a small cutoff length *a* has been introduced for the summation of ES interactions.

The minimization of the free energy difference $\Delta G(L)$ with respect to the fractions $\alpha_{c,r}$ yields the adsorption isotherm for counterion binding onto PE rings, as a transcendental equation for unknown α_c parameter,

$$\frac{\alpha_c}{1-\alpha_c}\frac{1-\alpha_r}{\alpha_r} = \exp\left[-\frac{l_B(\alpha_c\varepsilon_c(L) - \alpha_r\varepsilon_r(L))}{k_BTLb}\right] \quad (6)$$

Its solution shows that the PE rings condense more cations than the linear PEs do, Figure 1, decreasing thereby the ES ring formation penalty, Figure 2. The effect is more pronounced for smaller PE rings, with higher ES bending energy costs.

A relatively small increase of CC degree on PE rings found above is consistent with the outcomes of theoretical modeling of CC on DNA circular arcs performed in ref 53. Namely, even for very tight PE circles with radii of about 30 Å and at very low salt amounts, the enhancement of CC predicted in that paper did not exceed about 2%, as compared to CC on linear PEs. On the contrary, for a close parallel approach of two parallel PE

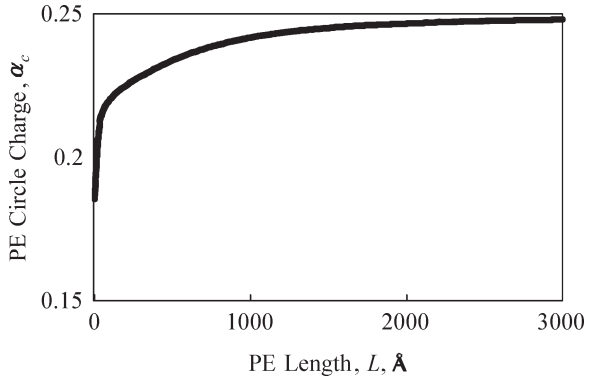

Figure 1. Fraction of non-neutralized charge on PE rings at low-salt conditions ($1/\kappa$ = 100 Å), for 75% of charge neutralized on a linear PE (α_r = 0.25), and cutoff length of a = 1 Å.

segments, the CC enhancement up to 15% has been detected, particularly when the PE surfaces were closer than the Debye screening length. Experimentally, the gel electrophoresis measurements on about kilo-bp long closed-circular supercoiled DNAs in mono- and di-valent salt solutions detected similar tendencies.[54] The DNA mobility analysis revealed that circular plasmid DNAs bind almost identical fraction of counterions from solution as the linear DNA fragments do.

For large ring radii R', the difference of the ring formation and ring closure energies asymptotes the Odijk−Skolnick−Fixman (OSF) ES PE bending energy[12,40] that is given for large rings by

$$\frac{E_{\mathrm{OSF}}}{k_{\mathrm{B}}T} \approx \frac{l_{\mathrm{p,OSF}}^{el}}{2}\frac{2\pi R'}{R'^2} \qquad (7)$$

The ES term in the total PE persistence length, $l_{\mathrm{p}} = l_{\mathrm{p}}^0 + l_{\mathrm{p}}^{\mathrm{el}}$, has a simple well-known form at low-salt conditions,

$$l_{\mathrm{p,OSF}}^{\mathrm{el}} \approx \frac{l_{\mathrm{B}}\alpha^2}{4\kappa^2 b^2} \qquad (8)$$

For DNA-relevant PE parameters, however, a stronger CC predicted by this model on PE rings only weakly affects the ES ring formation energies, Figure 2. We postulated that initially only 25% of PE charge was not neutralized by the condensed cations, the value relevant for the B-DNA in 1:1 simple salt solutions.[9,41]

There are several shortcomings in this simple physical model. First, the cutoff length a implemented has some effect on final results (smaller a values yield smaller variations in the ring charge density with ring radius). This a-dependence however largely drops out in the final solution for the ES ring formation energy. Second, the degree of CC on the rod, α_r, is an input parameter of the model and is not obtained self-consistently. Third drawback is that in the limit of $n_0 \to 0$ one can expect the tendencies of CC onto small circles to resemble those onto small spheres, that exhibit a weaker CC as compared to linear PEs.[11,42] The shape effects of circular PEs are however not taken account properly in this model. As a result, for the PE rings of all sizes, the current approach predicts an enhancement of CC that gives rise to a physically reasonable reduction of the ES energy of ring formation. Note that a stronger CC can be theoretically expected also for PE−PE dimer formation reaction, considered in Section 4.2, that would similarly diminish the ES penalty for the PE dimer formation.

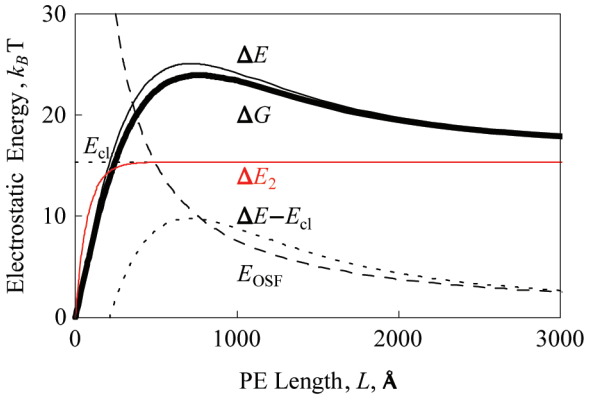

Figure 2. The ES energy [eq 2, thin curve] and free energy [eq 1, thick solid curve] of the ring formation, the ring closure energy [eq 3], the bending energy from the OSF theory [eq 7, dashed curve]. The ES dimerization energy ΔE_2 of PE fragments of length L is shown as the red curve. Parameters are the same as in Figure 1.

3. ELECTROSTATIC EFFECTS IN DNA CYCLIZATION

In this section, we analyze some physical implications of ES energies of PE ring and dimer formation on the cyclization probabilities of relatively short DNA fragments. The outcomes of our reaction-based approach for the ES J-renormalization are compared to the predictions based on the OSF theory of PE persistence.

3.1. Neutral Semiflexible Chains. Statistical properties of spontaneous cyclization of fluctuating semiflexible neutral polymer chains in solution have been thoroughly investigated long ago in the classical SY-study.[30] Namely, the molar J-factor that characterizes the local concentration of one end of the polymer in the vicinity of its another end, has been calculated. For relatively short polymer chains cyclized in solution so that the tangents on their ends are parallel, the cyclization probability follows a simple law:

$$J_{\mathrm{M}}(L) = \frac{J_{\mathrm{SY}}(L)}{(2l_{\mathrm{p}}^0)^3 N_{\mathrm{A}}} \sim 10^3 \frac{32\pi^3 l_{\mathrm{p}}^6}{L^6 (l_{\mathrm{p}}^0)^3} \exp\left[-\frac{2l_{\mathrm{p}}\pi^2}{L} + \frac{L}{4l_{\mathrm{p}}}\right] \qquad (9)$$

The polymer cyclization frequency depends exponentially on the mechanical bending energy stored in the ring (the first term in the exponential), being maximal for the chain length of $L \approx 3.3 l_{\mathrm{p}}$ or for ~500 bp DNA fragments. This energy term dominates the cyclization probability for short fragments. The L-dependent pre-exponential factor in eq 9 stems from chain fluctuations around the shape of a planar ring. The SY results are normalized here using the bare DNA persistence length l_{p}^0, the $(l_{\mathrm{p}}^0)^3$ term in the denominator.

This expression is valid for 2D polymer rings and it does not include the torsional energy required to align DNA ends in a helical register (i.e., effectively $l_{\mathrm{tw}} = 0$). The latter would result in regular oscillations of the J-factor below the SY curve, with the period of DNA helical repeat of ~10.5 bp and with the amplitude decreasing with the chain length.[30]

Equation 9 is not applicable to large circles, when polymer fluctuations (see refs 55 and 56), nonplanar ring shapes, and chain excluded-volume effects become progressively important. A typical scaling dependence that is realized for a long Gaussian polymer is $\propto L^{-3/2}$.[1] Accurate result follows from the second Daniels approximation for the cyclization of long semiflexible chains,

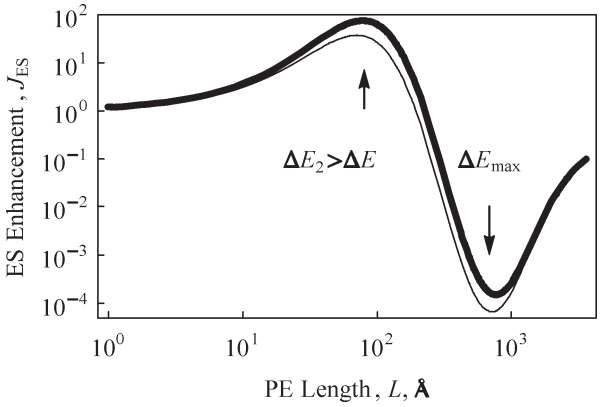

Figure 3. ES "enhancement" factor 13 exhibits a minimum for the chain length $L \approx 2\pi\lambda_D$ that corresponds to the strongest ES suppression of the J-factor. Parameters are the same as in Figure 1.

see eqs 59 and 60 of ref 29:

$$J_{M,\,\mathrm{Daniels}}(L) \approx \frac{10^3}{8l_p^3}\left(\frac{3}{2\pi(L/2l_p)}\right)^{3/2}\left(1-\frac{5}{8}\frac{2l_p}{L}-\frac{79}{640}\left(\frac{2l_p}{L}\right)^2\right) \tag{10}$$

Although we focus below on ES effects for relatively short chains, physically, for long PEs one can expect that at low n_0 the cyclization should also be suppressed by ES repulsions within the chain. This effect resembles a reduction of the knot formation probability by kbp-long DNAs at low-salt conditions, systematically studied and rationalized in ES terms in ref 43.

3.2. Renormalization of *J*: Reaction-Based Approach. An intuitive way to include the effects of ES ring closure energy on the formation of DNA cycles in solution is as follows. The J-factor is the ratio of the rate constants for monomolecular cyclization and bimolecular end-to-end association reactions[18]

$$J = k_1/k_2 \tag{11}$$

These constants can be regarded as exponential functions of the activation energy of the corresponding reactions. The ES energy for the circle formation ΔE is described by eq 2, while the ES dimerization energy of connecting two charged rods of length L into one piece of the length $2L$, is as follows:

$$\Delta E_2(L) = \frac{l_B\alpha^2}{2b^2}[\varepsilon_r(2L) - 2\varepsilon_r(L)] \tag{12}$$

The ratio k_1/k_2 is then renormalized by ES repulsions within PE rings and in PE dimers in an Arrhenius-like fashion

$$\frac{k_1}{k_2} \to \frac{k_1}{k_2}\exp\left[-\frac{\Delta E - \Delta E_2}{k_BT}\right] \equiv \frac{k_1}{k_2}J_{ES} \tag{13}$$

In this approximation, the SY J-factor is evaluated for the DNA mechanical persistence length, l_p^0, being then multiplied by ES suppression/enhancement factor J_{ES}. This is the main target quantity of the current study, evaluated here theoretically and contrasted against the outcomes of computer simulations in Section 4. It is important to mention that in this procedure the ES closure energy E_{cl} defined by eq 3 largely drops out in the final result for J_{ES} plotted in Figure 3.

This approach predicts that for large circles with radii $R' \gg \lambda_D$ the J-value approaches the SY prediction for neutral chains

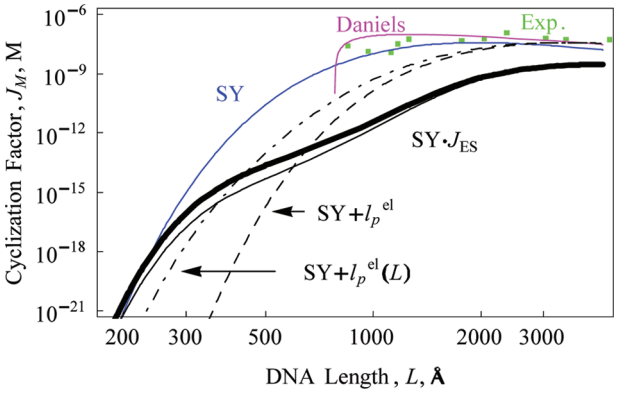

Figure 4. Molar cyclization factors J_M. The SY result with DNA mechanical persistence length only $l_p \equiv l_p^0 = 500$ Å (blue curve), with $l_p = l_p^0 + l_{p,OSF}^{el}$ (dashed curve), with $l_p = l_p^0 + l_p^{el}(L)$ [eq 14, dot-dashed curve]. The results of $k_{1,2}$-based renormalization according to eqs 9 and 13 with the ES energy and free energy of ring formation are shown as thin and thick solid curves, correspondingly. The green dots are the experimental data from Figure 5 of ref 18. The magenta curve is the theory limit for long neutral chains, eq 10. Other parameters are the same as in Figure 1.

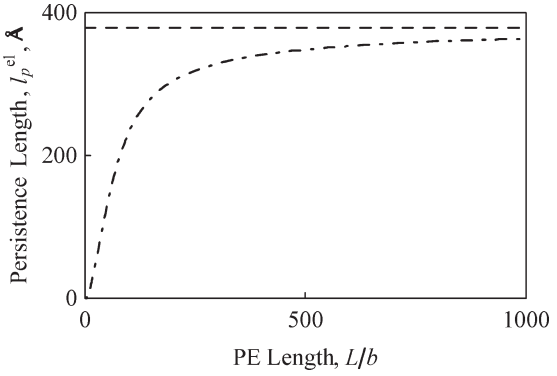

Figure 5. The ES persistence length of finite-length PE chains [eq 14, dot-dashed curve] and the OSF result for infinitely long PEs [eq 8, dashed curve]. Parameters are the same as in Figure 1.

from below, see Figure 4. In large-ring limit, the ES energy of end-to-end stacking of two PE fragments and of forming a ring from a single PE are nearly identical. The cyclization of medium-size rings, $R' \approx 1/\kappa$, is moderately ES-suppressed with $J_{ES} < 1$ in this case. This region corresponds to a maximum of ES ring energy $\Delta E(L)$ realized at $R' \approx \lambda_D$. We emphasize that for weakly screened ES repulsions (smaller κ values), the ES-renormalized J-factor deviates stronger from the SY result. Most importantly, for longer Debye lengths the region of maximal J-suppression shifts toward longer DNA fragments that can be an experimentally testable prediction.

For very small circles, $R' \ll 1/\kappa$, the ES-renormalized J-factor approaches the SY result as well, while in the region $2\pi R' \sim \lambda_D$ the ES suppression turns into the enhancement. This counterintuitive behavior emerges because for such small rings $\Delta E_2 > \Delta E$, see Figure 2. Physically, for very short PEs, twice as many charges participate in efficient ES interactions upon PE dimerization than during the PE ring formation. Thus, for small DNA rings the J-factors are expected to be enhanced and $J_{ES} > 1$ in this case, Figure 3.

To summarize, we predict a strong effect of PE ring formation and dimerization energies onto PE cyclization. The main

dx.doi.org/10.1021/jp2003479 |J. Phys. Chem. B 2011, 115, 4286–4294

message is a strong ES suppression of PE cyclization for PE lengths relevant to DNA cyclization experiments, ~100−1000 bp. Note also that a stronger CC on small PE rings predicted in the previous section affects the *J*-values rather marginally, compare the solid curves in Figure 4. Although an alternative model to account for ES effects in PE cyclization is presented below, the current reaction-based approach for ES renormalization of the *J*-factors is more physical.

Let us now dwell on some approximations employed above. We assumed for example that the pre-exponential factors in the expressions for $k_{1,2}$, describing the frequency to encounter a proper PE conformation in solution, are independent of intra- and inter-PE ES repulsions. To what extent this hypothesis is applicable to thermally-driven DNA ring and dimer formation in electrolyte solutions is rather hard to assess. Namely, the probability of end-to-end encounter of two PEs in solution is likely suppressed by their repulsion at low salt amounts. The kinetics of this reaction is also influenced by distance- and angle-dependent ES potentials for real DNA fragments.[44,45] The entire problem of DNA/PE cyclization is a difficult, yet unsolved theoretical task and the current study is an attempt to infer the ES effects for some ideal scenarios.

3.3. Renormalization of *J*: Persistence Length. Another way to incorporate the ES effects into the PE cyclization kinetics is to use the total DNA persistence length $l_p = l_p^0 + l_p^{el}$ in the SY expression 9 for uncharged chains. Such limit clearly neglects the ES ring and dimer formation energies, accounting only for bending of semiflexible PEs in electrolyte solution. For a PE of length $L = Nb$ at arbitrary salt conditions, the expression for the ES term $l_p^{el}(L)$ becomes more complicated that the classical result 8. Namely, the summation of the Debye−Hückel repulsions over a finite number N of charges on a weakly bent PE chain gives,

$$l_p^{el}(N) \approx \frac{l_B}{12Nb}\sum_{i=1}^{N-1}\sum_{j=i+1}^{N} e^{-\kappa b(j-i)}(1+\kappa b(j-i))b(j-i)$$

$$= \frac{l_B e^{-\kappa bN}}{12N(e^{\kappa b}-1)^4}\begin{bmatrix} e^{3\kappa b}(1+\kappa b+N+2\kappa bN+\kappa bN^2+e^{\kappa bN}(-1+N-\kappa b+\kappa bN))+ \\ e^{2\kappa b}(-2N+4\kappa b-2\kappa bN^2+e^{\kappa bN}(-2N-4\kappa b))+ \\ e^{\kappa b}(-1+\kappa b+N-2\kappa bN+\kappa bN^2+e^{\kappa bN}(1+N-\kappa b-\kappa bN)) \end{bmatrix} \quad (14)$$

At small κ values, this expression behaves similar to the length-dependent OSF result,

$$l_{p,OSF}^{el}(N) \approx \frac{l_B\{e^{-\kappa bN}[(\kappa bN)^2+5\kappa bN+8]+3\kappa bN-8\}}{12\kappa^3 b^3 N} \quad (15)$$

These two expressions start to deviate only at $1/\kappa \lesssim 3$ Å, while for the parameters of Figure 5 they nearly coincide. Note however that for long PE chains our eq 14 approaches the limit

$$l_{p,OSF}^{el}(\kappa) \approx \frac{l_B e^{\kappa b}(-1+\kappa b+e^{\kappa b}+\kappa b e^{\kappa b})}{12(e^{\kappa b}-1)^3} \quad (16)$$

that is valid at any salt concentration (within the limits of applicability of the OSF theory itself). The OSF length-dependent result eq 15 on the contrary turns into the low-salt limit of eq 8 for long chains. As the PE chain becomes longer, $L \gg \lambda_D$, the ES repulsions along it accumulate and the length-dependent persistence length approaches the result for the infinite PEs, see Figure 5.

The dot-dashed curve in Figure 4 for the ES-renormalized *J*-factor corresponds to the SY expression 9 with the persistence length $l_p = l_p^0 + l_p^{el}(L)$ with the ES term defined by eq 14. For large circles, this modified *J*-factor is slightly larger than the SY prediction for the uncharged chains (the blue curve). The physical reason for this fact is that the SY *J*-factor reaches a maximal for the chain length $L \approx 3.3l_p$. As PE chains with the ES term are more persistent, the maximum of *J*-factor shifts in the direction of longer chains. For small rings and low n_0, the renormalized $J(l_p^{el}(L))$ values are much lower than the SY prediction. The results for *J*-renormalization with the simple OSF $l_{p,OSF}^{el}$ persistence length are shown in this figure only for comparison (it gives a strong underestimation of *J*-values for small PE rings). As ES effects become progressively weaker at larger n_0 values, the ES contribution l_p^{el} to the total DNA persistence length reduces and the ES-renormalized *J*-factors approach the SY result for uncharged chains (data not shown).

4. RESULTS OF COMPUTER SIMULATIONS

In this section, we present some results of simple computer simulations aimed at a better understanding of ES effects in cyclization of semiflexible fluctuating PEs and compare them with the outcomes of an ideal model from Section 3.

4.1. Statistical Properties of Chains Generated. We have generated large assemblies (up to $M = 10^5$ chains) of semiflexible DNA-like PE chains of different lengths on the bp-level. The fluctuations of bp-variables are normally distributed as prescribed by the chain statistics at equilibrium. These bp variations mimic DNA thermal fluctuations in solution and characterize the energetic cost of bent DNA conformations. Namely, the twist τ, roll ϕ, and tilt Θ angles on every DNA bp are distributed according to the distribution functions,

$$f(\Theta,\phi) \propto \exp\left[-\frac{\Theta^2}{2\sigma_\Theta^2}\right]\exp\left[-\frac{\phi^2}{2\sigma_\phi^2}\right] \quad (17)$$

$$f(\tau) \propto \exp\left[-\frac{(\tau-\tau_0)^2}{2\sigma_\tau^2}\right] \quad (18)$$

Here, the we set the statistical parameters $\sigma_\Theta = \sigma_\phi$, $\sigma_\Theta{}^2 + \sigma_\phi{}^2 = 2l_0/l_p$, $\sigma_\tau{}^2 = l_0/l_{tw}$, with $l_0 = 3.4$ Å being the DNA rise per bp and $\tau_0 \approx 2\pi/10.5$ being the DNA average twist angle per bp. Below, we keep the notations for DNA bending $l_p \approx 500$ Å and twisting $l_{tw} \approx 750$ Å persistence lengths. In this procedure, the entire DNA chain is constructed from the initial tangent vector via applying the rotation matrix consecutively at every bp step, with the distribution functions defined by eqs 17 and 18. The chain generation procedure is described in great detail in ref 34.

We neglect here the possible effects of DNA charge symmetry and distribution of adsorbed cations on DNA onto intra-DNA ES

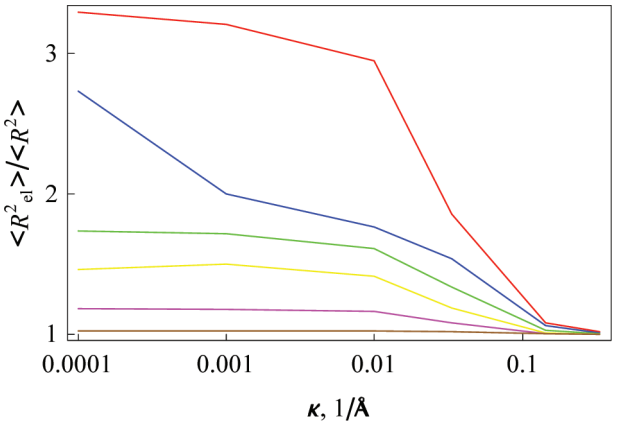

Figure 6. Swelling ratio of PE chains as computed from simulations according to eq 21. Color coding is the same as in Figure 7.

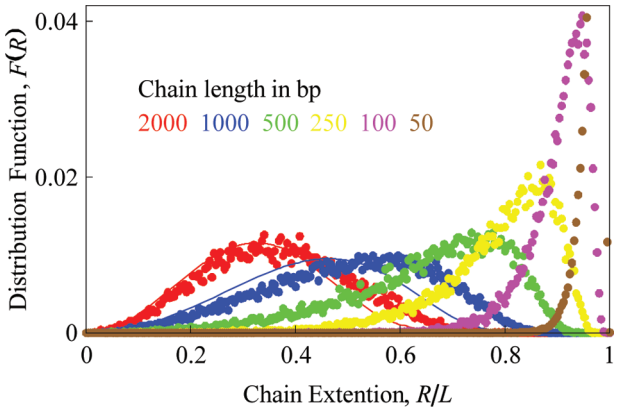

Figure 7. The radial distribution function as extracted from simulations (dots) and the theoretical predictions for semiflexible chains [eq 32 of ref 47; the curves with the corresponding color are plotted for long chains, $L/l_p \gg 1$, at l_p = 500 Å]. The chain extension region is divided into 250 segments, each represented by a point in the graph. For 50 bp long chains, the entire peak of $F(R)$ is not shown.

interactions, see ref 46. We position an effective point-like charge of magnitude $2e_0(1-\theta)$ every bp along the DNA axis. A typical value of $\theta = 0.8$ is used below as the DNA charge compensation fraction, for all chain lengths and salt concentrations. In the light of theoretical predictions from Section 2, one can expect this PE charge neutralization fraction to increase slightly for small circles at low salt levels. At more experimentally relevant conditions, however, the effect of this enhanced CC is expected to be rather small.

We compute the ES energy stored in the chain number m as a sum of Debye−Hückel repulsions over all pairs of charges,

$$E_{\mathrm{el,m}} = \frac{1}{2} k_B T l_B (2(1-\theta))^2 \sum_{\substack{(i,j)=1 \\ i \neq j}}^{N} \frac{e^{-\kappa r_{ij}}}{r_{ij}} \qquad (19)$$

Here, r_{ij} is the separation between charges i and j and N is the number of chain monomers. Particularly for long chains at low salt, this summation becomes computationally costly for large assemblies of $\sim 10^5$ chains. From the ES energy of fluctuating PEs, the energy of a straight rod E_r is subtracted in order to compute the excess ES energy of a fluctuating PE chain,

$$\Delta E_{\mathrm{el,m}} = E_{\mathrm{el,m}} - E_r \qquad (20)$$

The ES-mediated swelling of PE chains in solution can be quantified through the ratio of average end-to-end distances for charged and uncharged chains. For the former, the average is then weighted with the corresponding ES excess energies for the conformation m as follows:

$$\frac{\langle R_{\mathrm{el}}^2 \rangle}{\langle R^2 \rangle} = \frac{\sum_{m=1}^{M} R_m^2 e^{-\Delta E_{\mathrm{el},m}/k_B T}}{\sum_{m=1}^{M} e^{-\Delta E_{\mathrm{el},m}/k_B T}} \Bigg/ \frac{\sum_{m=1}^{M} R_m^2}{M} \qquad (21)$$

where M is the total number of chains in simulations. Intrachain ES repulsions govern the PE expansion, which is particularly pronounced for long PEs at low-salt conditions, see Figure 6.

From simulations, the radial distribution function $F(R)$ for the chains with a particular end-to-end distance R can also be restored. Figure 7 shows that in the limit $L/l_p \gg 1$ this distribution can be qualitatively described by the theoretical expression derived for semiflexible chains in ref 47:

$$F(R) \propto 4\pi R^2 (1-(R/L)^2)^{-3/2} (2-(R/L)^2)^{-3} \exp\left[-\frac{3L/(2l_p)}{2(1-(R/L)^2)}\right] \qquad (22)$$

According to it, the function $F(R)$ has a maximum at some chain extension, and it approaches zero for completely stretched and coiled chains. This maximum describes the most probable chain extension. The maximum shifts from the R/L value close to the full extension for short chains ($L \ll l_p$) to progressively smaller R/L for longer fragments. The peak is sharp for short chains that adopt nearly straight conformations and it widens for longer fragments that reveal in simulations much larger variations of shapes.

4.2. Electrostatics of Ring and Dimer Formation. The distribution of extensions and shapes of fluctuating PEs defines the distribution of the excess ES energy ΔE_{el}, see Figure 8. It illustrates that for longer PEs the ES energy distribution is wider and the average energy is larger, which is not surprising. Fitting the $\Delta E_{\mathrm{el}}(R/L)$-dependence down to the $R \to 0$ state, the ES penalty for nearly closed chain conformations can be extracted, Figure 9. In this figure, the entire range of chain extensions was divided into 150 intervals, each represented by a point of the average energy $\langle \Delta E_{\mathrm{el}} \rangle$ for a particular R/L value. As one could expect, longer chains possess many more states with spatially close ends, while for ~100 bp long chains the fraction of nearly closed states is extremely small. Thus, to extract some meaningful values of the ES ring formation energy, we analyze $\sim 10^5$ realizations for ~30 bp chains, as compared to $\sim 2 \times 10^4$ for longer fragments, for every κ value shown. In simulations, no condition of parallel tangents on the chain ends for ring-like chain conformations is imposed.

Figures 9, 10 show that the distribution of $\Delta E_{\mathrm{el,m}}$ generated appears to be more dispersed at smaller κ and smaller R/L values. Physically, at these conditions, relatively small variations of the PE shape might cause large changes in its ES energy. This fact complicates the precise evaluation of the closure energy ΔE for almost vanishing chain extension $R/L \to \Delta L/L \approx 0$. Particularly for <100 bp chains, the final ES ring formation energy depends

dx.doi.org/10.1021/jp2003479 |J. Phys. Chem. B 2011, 115, 4286–4294

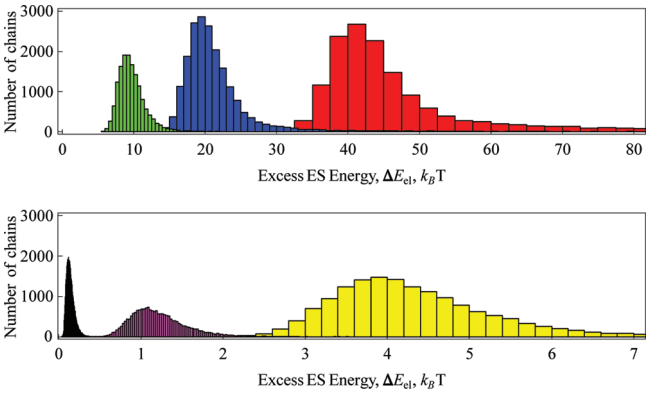

Figure 8. Distribution of the excess ES energy for the PE chains generaged. Color coding is the same as in Figure 7. The sample contains $\sim 2 \times 10^4$ chains. Parameters: $\theta = 0.8$ and $\lambda_D = 100$ Å.

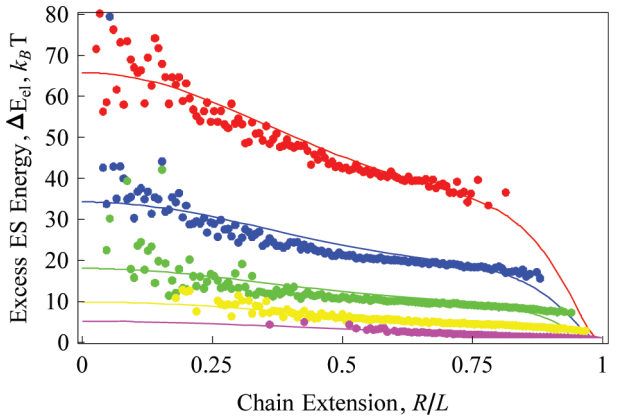

Figure 9. Extrapolating the ring closure energy ΔE from $\Delta E_{el}(R/L)$ distribution. Color scheme is the same as in Figure 7 and $1/\kappa = 100$ Å.

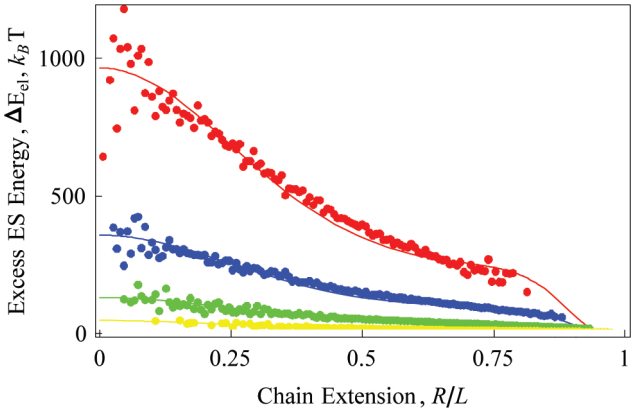

Figure 10. The same as in Figure 9 but at $1/\kappa = 1000$ Å.

strongly on the data-fitting method used. To avoid overestimated ΔE values for very short PEs, the fitting function $\beta_1[1-(R/L)^2]^p \mathrm{Exp}[-\beta_2(R/L)^4]$ with the fitting parameters $\beta_{1,2}$ has been implemented, instead of a simple exponential fit. We used the values $p = 2$ for $1/\kappa < 100$ Å, $p = 4$ for $1/\kappa = 200$ Å, and $p = 6$ for $1/\kappa > 200$ Å. Although this fitting function does account for a vanishing excess ES energy of stretched chains, this procedure remains the major source of inaccuracy in interpretation of simulation data for nearly closed PE conformations. The main

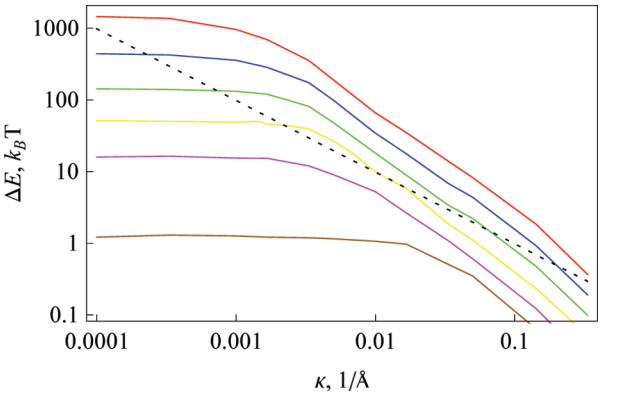

Figure 11. Average ES energy of closed PE conformations obtained from simulations. Color coding is the same as in Figure 7. Dependence of E_{cl} from eq 3 is shown as the black dotted line.

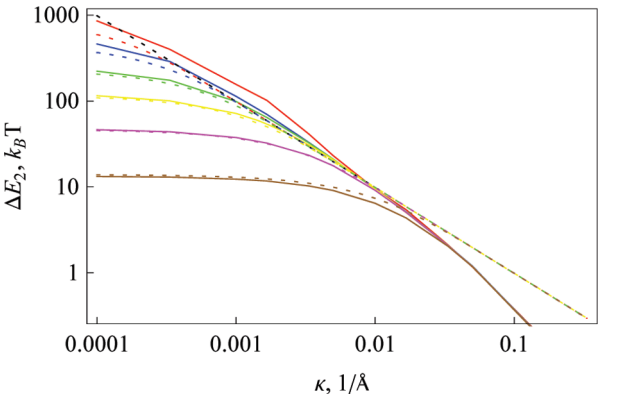

Figure 12. Average ES energy of PE dimer formation, as obtained from simulations (solid curves) and as predicted by theoretical model [eqs 5 and 12, colored dotted curves]. Black dotted curve is E_{cl}. The sampling contains at least $\sim 10^4$ chains for every chain length and κ value. Color coding is the same as in Figure 7 and $\Delta L \approx 0.1$ bp.

reason is that close-end polymer states are very sparsely populated especially for short chains. The final results for the ES ring formation energy of fluctuating PEs are presented in Figure 11.

Now, we enumerate the ES dimer formation energy, generating an assembly of two fluctuating PEs of the length L positioned at a small end-to-end distance ΔL. Starting with parallel tangents on the chain ends, we construct an assembly of chains growing in the opposite directions from the contact point, and then compute their mutual Debye−Hückel ES repulsions. The average dimer formation energy $\langle \Delta E_2 \rangle$ over all PE conformations involves the Boltzmann factor, $\langle \Delta E_2 \rangle = \Sigma_{m=1}^{M} \Delta E_{2,m} e^{-\Delta E_{2,m}/k_BT} / \Sigma_{m=1}^{M} e^{-\Delta E_{2,m}/k_BT}$, and the results are shown in Figure 12.

We observe that at large κ values, the dimerization energy collapses onto a universal curve for all chains. The physical reason for this is that in this limit, only the first two charges near the contact make a sizable contribution to ΔE_2. The analytical predictions for ES dimerization energy given by eqs 5 and 12 reveal a good agreement with the simulation results at intermediate-to-low salt concentrations, compare the solid and dashed curved in Figure 12. At large salt concentrations, however, the simulational results are appreciably lower than the theoretical predictions of ref 15. One possible reason is charge discreteness effects in simulations.

dx.doi.org/10.1021/jp2003479 |J. Phys. Chem. B 2011, 115, 4286–4294

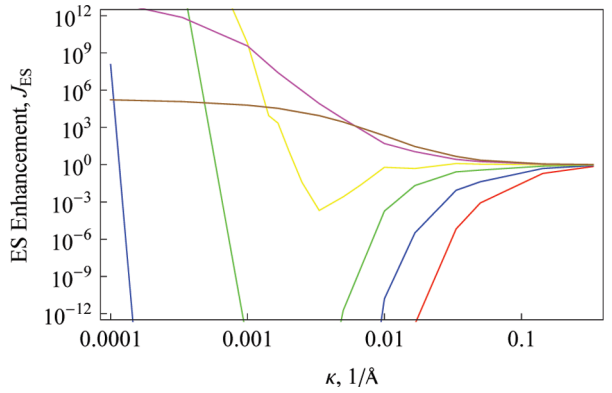

Figure 13. ES *J*-enhancement factor obtained from simulations. Color scheme is the same as in Figure 7.

We point out here that the minimal distance between the chain ends for PE rings and PE dimers is a natural important parameter, being set to $\Delta L = 0.1$ bp in simulations. We checked that smaller ΔL provide better agreement for ΔE_2 with the analytical results of *R*. Netz given by eq 5, particularly at low salt. At larger κ values, the simulation results for ΔE_2 decrease however more rapidly than the $\propto 1/\kappa$ law prescribed by eq 3. When larger ΔL values are used in modeling, the energy ΔE_2 is underestimated for the Debye lengths < ΔL.

The calculated ES energies of the ring and dimer formation are now inserted into the ES enhancement factor, eq 13. For long PEs, a gigantic suppression of cyclization is observed for $\lambda_D \sim 30-1000$ Å. Only at extremely low salt conditions, this suppression turns into an enhancement, see the behavior of the blue curve in Figure 13 representing 1000 bp long chains. The point of this low-salt suppression-to-enhancement transition shifts toward larger κ values as the PE chains become shorter (as one can see contrasting the blue to green to yellow curve behavior in Figure 13). This is an important message from simulations.

For the chains shorter than $\sim\lambda_D$, the cyclization reaction can be stimulated because the ring formation is less ES-costly than PE dimerization. The physical explanation is again a "doubling" of strongly repelling charges on PE dimers as compared to PE rings. For 50 and 100 bp long chains, we detected an enhancement in the entire range of salt concentrations studied. For the chain length of 500 bp, the simulations predict a strong enhancement at $\lambda_D \gtrsim 1000$ Å and a strong-to-moderate suppression at continuously growing salt concentrations. The ES enhancement factor exhibits a nonmonotonic dependence with a minimum, as a function of added simple salt.

Similar to the theoretical predictions, for intermediate chain lengths a maximal *J*-suppression in simulations occurs for ring radii of $R' \approx \lambda_D$. The magnitude of these ES effects naturally diminishes with the addition of salt, together with the corresponding energies ΔE and ΔE_2. A large discrepancy is observed however for long chains. Namely, contrary to the model predictions for ideal PE rings shown in Figure 2, the cyclization and dimerization energies obtained from simulations do not equalize for long fluctuating PEs. This fact causes in particular a dramatic suppresion of *J*-factors of thermally-agitated PEs longer than about 500 bp in a broad range of salt concentrations, see Figure 13.

At a constant $\lambda_D = 100$ Å value, as the chain length decreases, we observe a transition from enormous *J*-suppression for 1000 and 2000 bp long chains, to a moderate suppression for ~500 bp chains, and eventually to a moderate enhancement for 30 and 100 bp long chains. It resembles the theoretical behavior illustrated in Figure 3.

5. DISCUSSION AND CONCLUSIONS

First, we list below the main salt-dependent features of the PE ring and dimer formation as obtained from a simplistic theoretical model developed. For the parameters relevant for DNA cyclization reaction, the enhanced CC on PE circles was shown to affect rather moderately the ES ring formation energy. The ES energies of ideal PE rings and linear PE dimers gave rise to a nonmonotonic behavior for the ES *J*−renormalization factor J_{ES}. The region of maximal *J*-suppression predicted for long PE chains was demonstrated to shift toward longer fragments at lower salt levels. For very short PEs, on the contrary, a relatively weak *J*-enhancement might occur, $J_{ES} > 1$. The goal of future theoretical studies is a formulation of exact functional-integral-based approach to a problem of cyclization of semiflexible PE chains, analogously to the SY theory for uncharged polymers.

The outcomes of our computer simulations of fluctuating PE chains support some of these theoretical tendencies. For instance, an enhancement of the *J*-factor is predicted for very short PEs 30−100 bp in the entire range of salinities studied, while for long chains, a suppression is found for almost all values of κ. At a physiological salt level of ~0.1 M, a quite weak ES-induced *J*−suppression is shown for intermediate-to-long chains, $J_{ES} < 1$, which turns into a weak ES enhancement for short PEs, see Figure 13. At such high salt levels, we expect only weak ES effects onto DNA cyclization. We argue that the concentrations of mono- and divalent salts are essential additional parameters that are likely to control the properties of DNA cyclization in solution. In particular, our theoretical and computational results indicate a strongest ES-induced suppression of PE/DNA cyclization for the ring size comparable to the Debye screening length, $R' \sim \lambda_D$, the main result of the paper.

In real DNA cyclization experiments, several factors can mask or overwhelm the ES effects of the simple salt anticipated above. Some of them are listed below. Still, we hope that future DNA cyclization expriments, performed particularly at very low salt amounts (unscreened Coulomb interactions), could validate whether the peculiar ES enhancement-suppression behavior predicted above is relevant for real DNA systems.

As mentioned in Introduction, the binding of T4 DNA ligase to DNA ends ensures a "trapping" of fluctuating molecules in solution provided their ends are spatially close enough. This reaction produces the distinct amounts of DNA rings and DNA dimers defining thereby the *J*-factor. The ligation reaction is much more efficient for DNA fragments with sticky/cohesive ends, as compared to DNAs with blunt ends. For sticky DNA ends, the situation typically implemented to measure the *J*-factors in experiments,[21,22] the ligase-mediated DNA-strand pairing is facilitated by a favorable chemical energy of joining the complementary single-stranded DNA ends. The blunt DNA ends lack this pairing energy and thus require much higher ligase concentrations to trigger a substantial yield of DNA with the joined ends. Note that the situation with non-cohesive ends is however closer to the model and simulation procedure performed above.

Another factor is that the presence of ~10 mM of $MgCl_2$ in DNA cyclization buffers ensures the efficient DNA end-joining reaction by T4 DNA ligase, while the levels of NaCl larger

than ∼200 mM are known to strongly inhibit this reaction.[48] Some trivalent cations (e.g., 1−5 mM of spermidine^{3+}) also strongly inhibit the DNA cyclization by T4 DNA ligase.[48] Experimentally, the effect of divalent cations on cyclization of ∼200 bp DNA fragments with short single-stranded gaps has been thoroughly studied in ref 23. It was observed in particular that a decrease of $MgCl_2$ concentration in the buffer from the standard 10 down to 1 mM gives rise to a notable decrease in the J−factor. This decrease has been attributed to an enhanced ES repulsion of neighboring double-stranded DNA segments in the vicinity of DNA−DNA junction point in these gapped DNA rings. The divalent cations often interact with DNA much more strongly and thus might mask the ES effects of monovalent salt on the formation of DNA rings and dimers predicted above.

On the DNA side, it is known that divalent Mg^{2+} cations can soften the double helix significantly, reducing its bending persistence length from ∼500 down to ∼250 Å.[37] We are however not aware of any systematic measurements of DNA persistence length at different amounts of Mg^{2+}in the buffer. This complicates the estimation of a proper value for DNA persistence length to be used in theoretical models and the interpretation of future experimental data on salt-dependent DNA cyclization.

It is important to mention that different levels of simple salt also affect the ligase-DNA binding activity itself. The presence of a positively charged cleft on DNA ligases in the pocket for DNA binding[49] is likely to impose some salt-dependence of (partly) ES-driven ligase-DNA binding. This necessitates a calibration of the ligase activity at different salt levels. At large ligase concentrations, that are required to catalyze the cyclization of short DNA fragments, the ligase-DNA binding might also trigger a DNA softening and thereby facilitate the formation of DNA rings.[50]

From the geometrical point of view, it has been argued that a nearly parallel alignment of DNA ends near the junction is a prerequisite for an efficient DNA ligation reaction. Crystal structures of DNA ligases also support this view of only slightly bent DNA at the site of ligase-DNA binding. Physically however, especially for DNA mini-circles, the mechanical bending energy to create an ideal circle is substantially larger than the minimal energy of a closed loop for the same chain length. This optimal form is known to have a tear-drop shape, minimizing the elastic energy in the linear elasticity theory.[29,52] The energetics of the ligase binding to close DNA ends is therefore also important to quantify in the future.

Last but not least, the integrity of DNA structure is a fundamental assumption in the model. However, when the mechanical and ES energies of the ring formation exceed $\sim 10-20 k_B T$, the defects in DNA structure might emerge as a response. Unpairing of DNA bases, formation of kinks, and melted bubbles in DNA[51] are some possible scenarios for small DNA rings. For instance, the formation of melted single-stranded DNA bubbles has been rationalized in ref 52 as a possible theoretical explanation for the abnormally high J-factors measured for ∼100 bp DNA fragments in ref 21.

Modifications of ES models of DNA cyclization that will account for these effects comprise possible directions for future theoretical research.

■ ACKNOWLEDGMENT

Many helpful discussions with R. Everaers and R. Winkler are gratefully acknowledged. Financial support from the German Research Foundation DFG made this work possible.

■ REFERENCES

(1) Rippe, K.; von Hippel, P. H.; Langowski, J. *Trends Biochem. Sci.* **1995**, *20*, 500.
(2) Towles, K. B.; et al. *Phys. Biol.* **2009**, *6*, 025001.
(3) Garcia, H. G.; et al. *Biopol.* **2006**, *85*, 115.
(4) Swigon, D.; Coleman, B. D.; Olson, W. K. *Proc. Natl. Acad. Sci. U.S.A.* **2006**, *103*, 9879.
(5) Balaeff, A.; Mahadevan, L.; Schulten, K. *Phys. Rev. E* **2006**, *73*, 031919.
(6) Cherstvy, A. G. *J. Phys. Chem. B* **2009**, *113*, 4242.
(7) Cherstvy, A. G. *Eur. Biophys. J.* **2011**, *40*, 69.
(8) White, C. L.; et al. *EMBO J.* **2001**, *20*, 5207.
(9) Manning, G. S. *Q. Rev. Biophys.* **1978**, *11*, 179.
(10) Manning, G. S. *Macromolecules* **2001**, *34*, 4650.
(11) Manning, G. S. *J. Phys. Chem. B* **2007**, *111*, 8554.
(12) Skolnick, J.; Fixman, M. *Macromolecules* **1977**, *10*, 944.
(13) Ariel, G.; Andelman, D. *Europhys. Lett.* **2003**, *61*, 67.
(14) Guo, Z.; et al. *J. Phys. Chem. B* **2008**, *112*, 16163.
(15) Kunze, K. K.; Netz, R. R. *Phys. Rev. E.* **2002**, *66*, 011918.
(16) Cherstvy, A. G. *J. Biol. Phys.* **2011**, *37*, 227.
(17) Shore, D.; Baldwin, R. L. *J. Mol. Biol.* **1983**, *170*, 957.
(18) Shore, D.; Langowski, J.; Baldwin, R. L. *Proc. Natl. Acad. Sci. U.S.A.* **1981**, *78*, 4833.
(19) Hagerman, P. J.; Ramadevi, V. A. *J. Mol. Biol.* **1990**, *212*, 351.
(20) Taylor, W. H.; Hagerman, P. J. *J. Mol. Biol.* **1990**, *212*, 363.
(21) Cloutier, T. E.; Widom, J. *Mol. Cell* **2004**, *14*, 355.
(22) Du, Q.; et al. *Proc. Natl. Acad. Sci. U.S.A.* **2005**, *102*, 5397.
(23) Du, Q.; et al. *Biophys. J.* **2005**, *88*, 4137.
(24) Cloutier, T. E.; Widom, J. *Proc. Natl. Acad. Sci. U.S.A.* **2005**, *102*, 3645.
(25) Douarche, N.; Cocco, S. *Phys. Rev. E* **2005**, *72*, 061902.
(26) Kahn, J. D.; Crothers, D. M. *Proc. Natl. Acad. Sci. U.S.A.* **1992**, *89*, 6343.
(27) Jacobson, H.; Stockmayer, W. H. *J. Chem. Phys.* **1950**, *18*, 1600.
(28) Gobush, W.; et al. *J. Chem. Phys.* **1972**, *57*, 2839.
(29) Yamakawa, H.; Stockmayer, W. H. *J. Chem. Phys.* **1972**, *57*, 2843.
(30) Shimada, J.; Yamakawa, H. *Macromolecules* **1984**, *17*, 689.
(31) Wilson, D. P.; et al. *Europhys. Lett.* **2010**, *89*, 58005.
(32) Wiggins, P. A.; et al. *Phys. Rev. E* **2005**, *71*, 021909.
(33) Wiggins, P. A.; et al. *Phys. Rev. E* **2006**, *73*, 031906.
(34) Levene, S. D.; Crothers, D. M. *J. Mol. Biol.* **1986**, *189*, 61.
(35) Podtelezhnikov, A. A.; Vologodskii, A. V. *Macromolecules* **2000**, *33*, 2767.
(36) Wiggins, P. A.; et al. *Nat. Nanotechnol.* **2006**, *1*, 137.
(37) Baumann, C. G. *Proc. Natl. Acad. Sci. U.S.A.* **1997**, *94*, 6185.
(38) Podesta, A.; et al. *Biophys. J.* **2005**, *89*, 2558.
(39) Widom, J.; personal communication, 2008.
(40) Odijk, T. *J. Polym. Sci.* **1977**, *15*, 477.
(41) Keyser, U. F.; et al. *Nature Physics* **2006**, *2*, 473.
(42) Le Bret anf, M.; Zimm, B. H. *J. Biomol. Struct. Dyn.* **1983**, *1*, 461.
(43) Vologodskii, A.; Cozzarelli, N. *Biopolymers* **1995**, *35*, 289.
(44) Brenner, S. L.; Parsegian, A. V. *Biophys. J.* **1974**, *14*, 327.
(45) Cherstvy, A. G. *J. Phys. Chem. B* **2008**, *112*, 12585.
(46) Cherstvy, A. G. *J. Phys. Chem. B* **2007**, *111*, 7914.
(47) Winkler, R. G. *J. Chem. Phys.* **2003**, *118*, 2919.
(48) Wu, D. Y.; Wallace, R. B. *Gene* **1989**, *76*, 245.
(49) Subramanya, H. S.; et al. *Cell* **1996**, *85*, 607.
(50) Yuan, C.; et al. *Nucleic Acids Res.* **2007**, *35*, 5294.
(51) Mitchel, J. S.; Laughton, C. A.; Harris, S. A. *Nucleic Acids Res.* 2011, DOI: 10.1093/nar/gkq1312
(52) Yan, J.; Marko, J. F. *Phys. Rev. Lett.* **2004**, *93*, 108108.
(53) Fenley, M. O.; et al. *Macromol.* **2000**, *33*, 1899.
(54) Ma, C.; Bloomfield, V. A. *Biopolymers* **1995**, *35*, 21.
(55) Fedorov, M. V.; et al. *J. Am. Chem. Soc.* **2009**, *131*, 10854.
(56) Fedorov, M. V.; et al. *Chem. Comm.* **2009**, *8*, 896.